Photocatalytic Water Splitting on Ni-Intercalated Ruddlesden−Popper Tantalate $H_2La_{2/3}Ta_2O_7$

Ken-ichi Shimizu,*,† Seiichiroh Itoh,‡ Tsuyoshi Hatamachi,§ Tatsuya Kodama,§ Mineo Sato,§ and Kenji Toda‡

Department of Applied Chemistry, Graduate School of Engineering, Nagoya University, Chikusa-ku, Nagoya 464-8603, Japan, Graduate School of Science and Technology, Niigata University, Ikarashi-2, Niigata 950-2181, Japan, and Department of Chemistry and Chemical Engineering, Faculty of Engineering, Niigata University, Ikarashi-2, Niigata 950-2181, Japan

Received May 11, 2005. Revised Manuscript Received July 12, 2005

A series of Ruddlesden−Popper-type hydrous layered perovskites, $A'_2ATa_2O_7$ (A′ = H or K, A = $La_{2/3}$ or Sr), were presented as novel catalysts for photocatalytic water splitting into H_2 and O_2 under UV irradiation. These hydrous perovskites showed higher activity than anhydrous perovskites ($KTaO_3$, $La_{1/3}TaO_3$) for overall splitting of water. Results of photoluminescence spectroscopy and H_2 evolution from aqueous *n*-butylamine solution support the hypothesis that the high activity of the hydrous perovskites results from their hydrated layered structure, where the photogenerated electrons and holes can be effectively transferred to the intercalated substrates (H_2O and *n*-butylamine). Addition of Ni cocatalyst to $H_2La_{2/3}Ta_2O_7$ via an ion-exchange reaction increased the activity, while Ni addition did not improve the activity of $H_2SrTa_2O_7$. Ni K-edge EXAFS/XANES, UV−vis spectroscopy, and TEM results for Ni-loaded catalysts indicate that Ni^{2+} ions and small NiO clusters are intercalated into the layers of $H_2La_{2/3}Ta_2O_7$, while relatively large NiO particles at the external surface of the perovskite are the main Ni species in $H_2SrTa_2O_7$. Thus, the highly dispersed Ni(II) species at the interlayer space are shown to act as effective sites for H_2 evolution in the photocatalytic water splitting.

Introduction

Much attention has been paid to the photocatalytic decomposition of water into H_2 and O_2 over semiconductor materials, as it can potentially provide a clean and renewable source for hydrogen fuel in the future. A variety of photocatalysts, mainly Ti-,[1−3] Nb-,[4,5] and Ta-based[6−13] oxides, have been reported to be effective for the photocatalytic decomposition of water. The group of Domen and coworkers[3−5] first demonstrated that hydrous layered oxides, $K_4Nb_6O_{17}$ and $K_2La_2Ti_3O_{10}$, show much higher activity for water splitting than the "bulk-type" catalysts such as Pt/TiO_2. It was proposed that these layered materials use their interlayer space as reaction sites, where the electron−hole recombination process could be retarded by physical separation of the electron and hole pairs generated by photoabsorption. On the other hand, bulk-type Ta-based oxides have been developed as a new class of photocatalyst.[6−11] Among these catalysts, La-doped $NiO/NaTaO_3$, developed by Kudo et al., shows the highest quantum yields under UV irradiation.[10]

Ruddlesden−Popper phases (RP), with the general formula of $A'_2[A_{n-1}B_nO_{3n+1}]$, are of great interest for their superior physical properties, such as ion-exchange, intercalation, and catalysis. Recently, several groups reported the synthesis, structure, and properties of a new $n = 2$ member perovskite tantalate, $A'_2ATa_2O_7$ (A′ = H or K, A = $La_{2/3}$ or Sr),[14−18] which is composed of layers of A−Ta perovskite sheets and A′ ions located in the hydrous interlayer. We have recently demonstrated the first successful example of active hydrous Ta-based photocatalysts, $A'_2SrTa_2O_7{\cdot}nH_2O$ (A′ = H, K, and Rb) as an effective photocatalyst for water splitting, though its modification by Ni cocatalyst results in a decrease in the activity as reported in this paper. We hypothesized that effective "two-dimensional" photocatalysts can be designed

* Corresponding author. Fax: +81-52-789-3193. E-mail: kshimizu@apchem.nagoya-u.ac.jp.
† Nagoya University.
‡ Graduate School of Science and Technology, Niigata University.
§ Department of Chemistry and Chemical Engineering, Niigata University.

(1) Domen, K.; Naito, S.; Onishi, T.; Tamaru, K. *Chem. Phys. Lett*. **1982**, *92*, 433.
(2) Inoue, Y.; Kubokawa, T.; Sato, K. *J. Chem. Soc., Chem. Commun*. **1990**, 1298.
(3) Takata, T.; Furumi, Y.; Shinohara, K.; Tanaka, A.; Hara, M.; Kondo, J. N.; Domen, K. *Chem. Mater*. **1997**, *9*, 1063.
(4) Kudo, A.; Sayama, K.; Tanaka, A.; Asakura, K.; Domen, K.; Maruya, K.; Onishi, T. *J. Catal*. **1989**, *120*, 337.
(5) Sayama, K.; Tanaka, A.; Domen, K.; Maruya, K.; Onishi, T. *J. Phys. Chem.* **1991**, *95*, 1345.
(6) Kudo, A.; Kato, H. *Chem. Lett*. **1997**, 867.
(7) Ishihara, T.; Nishiguchi, H.; Fukamachi, K.; Takita, Y. *J. Phys. Chem. B* **1999**, *103*, 1.
(8) Kudo, A.; Kato, H.; Nakagawa, S. *J. Phys. Chem. B* **2000**, *104*, 571.
(9) Kato, H.; Kudo, A. *J. Phys. Chem. B* **2001**, *105*, 4285.
(10) Kudo, A.; Asakura, K.; Kato, H. *J. Am. Chem. Soc*. **2003**, *125*, 3082.
(11) Zou, Z.; Ye, J.; Sayama, K.; Arakawa, H. *Nature* **2001**, *414*, 625.
(12) Machida, M.; Yabunaka, J.; Kijima, T. *Chem. Mater*. **2000**, *12*, 812.
(13) Shimizu, K.; Tsuji, Y.; Hatamachi, T.; Toda, K.; Kodama, T.; Sato, M.; Kitayama, Y. *Phys. Chem. Chem. Phys.* **2004**, *6*, 1064.
(14) Bhuvanesh, N. S. P.; Crosnier-Lopez, M. P.; Duroy, H.; Fourquet, J. L. *J. Mater. Chem*. **1999**, *9*, 3093.
(15) Crosnier-Lopez, M. P.; Le Berr, F.; Fourquet, J. L. *J. Mater. Chem*. **2001**, *11*, 1146.
(16) Crosnier-Lopez, M. P.; Le Berr, F.; Fourquet, J. L. *Z. Anorg. Chem*. **2002**, 2049.
(17) Olliver, P. J.; Mallouk, T. E. *Chem. Mater*. **1998**, *10*, 2585.
(18) Schaak, R. E.; Mallouk, T. E. *Chem. Mater*. **2000**, *12*, 3427.

10.1021/cm050982c CCC: $30.25
Published on Web 08/27/2005

if the Ni cocatalyst is intercalated into this type of layered tantalate, as successfully demonstrated for the layered niobate system.[4,5] In this paper, we report the first successful example of highly active Ni-intercalated layered tantalate photocatalysts with hydrated interlayer space. The effect of the hydrous interlayer on the photocatalytic efficiency is discussed on the basis of the results of photoluminescence spectroscopy and the hydrogen evolution from an aqueous solution of *n*-butylamine. The Ni-loaded catalysts are characterized by XRD, UV−vis spectroscopy, XAFS, and TEM to discuss the influence of the state of the Ni on the activity.

Experimental Section

Catalyst Preparation and Characterization. $K_2La_{2/3}Ta_2O_7$ powders were prepared by a conventional solid-state reaction following the method by Crosnier-Lopez et al.[16] Stoichiometric amounts of La_2O_3 and Ta_2O_5 with a 67% molar excess of K_2CO_3 were mixed together, pressed into pellets, and heated in air at 1073 K for 6 h and then at 1498 K for 15 h. K^+/H^+ exchange of $K_2La_{2/3}Ta_2O_7$ (1.0 g) was performed using 200 mL of 1 M HNO_3 at room temperature (24 h), and the sample was washed with deionized water and dried in vacuo at 298 K (20 h). Dehydration of $H_2La_{2/3}Ta_2O_7$ by heating at 1273 K for 6 h resulted in the formation of a solid mostly composed of $La_{1/3}TaO_3$ (JCPDS 42-0061) as described later. $H_2SrTa_2O_7$[13] was prepared by the K^+/H^+ exchange of $K_2SrTa_2O_7$,[15] prepared by a solid-state reaction of $SrCO_3$, Ta_2O_5, and K_2CO_3 at 1173 K. Ni-loaded catalyst was prepared by an impregnation of H^+-exchanged sample (1.0 g) with an aqueous solution (20 mL) of $Ni(NO_3)_2 \cdot 6H_2O$ (Wako Pure Chemical; 98.0%). After stirring for 1 h, the water was evaporated on a water bath. The powder was dried at 353 K for 4 h and then calcined at 573 K for 1 h in air.

The crystal structure of the obtained material was confirmed by X-ray diffraction (MAC Science; MX Labo) with Cu Kα radiation (40 kV, 25 mA) at room temperature. Transmission electron microscopy (TEM) was carried out on a JEOL JEM-2010 operating at 200 kV. Thermogravimetric (TGA) analysis coupled with differential thermal analysis of the hydrated oxides was made using an MTC1000 (MAC Science) operating with a heating rate of 10 K min^{-1}. Diffuse reflectance spectra were obtained with a UV−vis spectrometer (Jasco; V-550) and were analyzed by the Kubelka−Munk method. The optical band-gap energy was calculated from onset of absorption edges. Photoluminescence was measured at 77 K using a closed quartz cell and a fluorometer (HITACHI F-4500). For $K_2SrTa_2O_7$ in anhydrous form, XRD, UV−vis, and photoluminescence measurements were carried out immediately after calcination in order to avoid the hydration process. Ni K-edge XAFS spectra were obtained at BL-7C (Photon Factory in High Energy Accelerator Research Organization, Tsukuba, Japan) with a Si(111) double-crystal monochromator. X-ray absorption spectra of the Ni-loaded photocatalysts were obtained in the fluorescent mode using a Lytle detector, whereas those of the reference Ni samples were obtained in a transmittance mode. The energy was defined by assigning the first inflection point of the Cu foil spectrum to 8980.3 eV. The EXAFS data were analyzed by the EXAFS analysis program REX version 2.5. The Fourier transforms of k^3-weighted EXAFS were typically obtained in the k range of 3−12 $Å^{-1}$. For the curve fitting analysis (in the R range of 3.4−11.5 Å) with Ni−O and Ni−Ni shells, empirically derived phase shift and amplitude functions extracted from $Ni(OAc)_2 \cdot 6H_2O$ and NiO were used, respectively.

Photocatalytic Reaction. The photocatalytic decomposition of water was performed with a closed gas circulating system. The catalyst powder (0.5 g) was dispersed in 200 mL of pure water by a magnetic stirrer in an inner irradiation cell made of quartz. The light source was a 400 W high-pressure mercury lamp. Before the reaction, the mixture was degassed completely, and then Ar (ca. 15 kPa) was introduced. The amounts of evolved H_2 and O_2 were determined by gas chromatography (Hitachi, TCD, molecular sieve 5A column and Ar carrier), the sampler (3 mL) of which was directly connected to the closed gas circulation system to avoid any contamination from air. Gas evolution was observed only under photoirradiation.

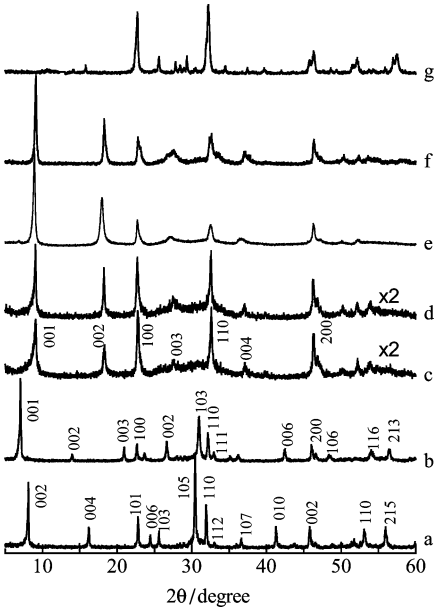

Figure 1. Powder X-ray diffraction patterns of (a) anhydrous $K_2La_{2/3}Ta_2O_7$, (b) $K_2La_{2/3}Ta_2O_7$, (c) $H_2La_{2/3}Ta_2O_7$ (d) NiO(2 wt %)−$H_2La_{2/3}Ta_2O_7$, (e) $H_2SrTa_2O_7$, (f) NiO(0.5 wt %)−$H_2SrTa_2O_7$, and (g) $La_{1/3}TaO_3$.

Results and Discussions

Characterization. The XRD pattern of $K_2La_{2/3}Ta_2O_7$ was recorded immediately after calcination (Figure 1a); all the observed lines could be indexed on a tetragonal cell (*I*4/*mmm*, $a = 3.9608$ Å, $c = 21.8126$ Å),[16] indicating that this compound consists of a single phase of layered perovskite, anhydrous $K_2La_{2/3}Ta_2O_7$. The structure of anhydrous $K_2La_{2/3}Ta_2O_7$ can be described as being formed from two TaO_6 octahedra thick slabs of a perovskite lattice cut along the *c* direction; these alternate layers are shifted by $(a+b)/2$ (body centered), with the large La cations occupying two-thirds of the 12-coordination sites. As Crosnier-Lopez et al.[16] reported, $K_2La_{2/3}Ta_2O_7$ allowed spontaneous intercalation of water; after exposing it to humid air for 1 h, the anhydrous form of $K_2La_{2/3}Ta_2O_7$ completely disappeared, and hydrous $K_2La_{2/3}Ta_2O_7$ (*P*4/*mmm*, $a = 3.9484$ Å, $c = 12.8049$ Å) appeared simultaneously. This structural change has been attributed to a shift of alternate layers; the adjacent layers are stacked immediately above each other in the same arrangement leading to a halving of the *c*-axis length upon hydration.[16] As previously reported,[13] $K_2SrTa_2O_7$ (*P*4/*mmm*, $a = 3.9974$ Å, $c = 12.133$ Å) also allowed spontaneous intercalation of water, though its hydration rate is much lower than that for $K_2La_{2/3}Ta_2O_7$. Figure 2 shows an increase in the relative line intensity due to the hydrous phase as a function of the time of exposure to humid air. The result

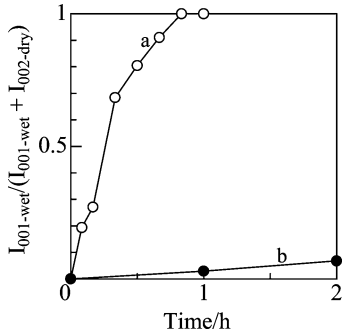

Figure 2. Changes in the ratio of XRD lines, $I_{001-\text{wet}}/(I_{001-\text{wet}} + I_{002-\text{dry}})$, for (a) $K_2La_{2/3}Ta_2O_7$ and (b) $K_2SrTa_2O_7$ after dehydration at 773 K for 2 h as a function of the time of exposure to humid air. $I_{001-\text{wet}}$ and $I_{002-\text{dry}}$ denote the height of the XRD lines due to (001) for the hydrous phase and (002) for the anhydrous phase, respectively. The XRD patterns were taken at room temperature.

Table 1. Physical Properties and Photocatalytic Activities of Various Perovskite-Type Tantalates

catalyst	n^a	band gap eV[b]	SBET $m^2\ g^{-1}$ [c]	evolution rate (mmol h^{-1}) H_2[d]	O_2[d]	$H_2(BuNH_2)$[e]	$[BuNH_2]$[f] mmol g^{-1}
$K_2La_{2/3}Ta_2O_7$	2.1	4.0	3.7	146	66	918	0.38
$H_2La_{2/3}Ta_2O_7$	1.0	4.0	7.8	158	77	2654	0.90
$La_{1/3}TaO_3$	0	4.0	3.3	35	7.9	424	0
$H_2SrTa_2O_7$	0.6	3.9	4.0	385	179	1490	0.94
$KTaO_3$	0	3.6	1.5	25	3.3	270	0.01

[a] Water content expressed as a molar ratio (mol/mol) estimated from TGA. [b] Estimated from the onset of absorption. [c] BET surface area estimated from N_2 adsorption. [d] Rate of H_2 or O_2 evolution from pure water (catalyst amount = 0.5 g). [e] Rate of H_2 evolution from an aqueous *n*-butylamine (0.25 M) solution (catalyst amount = 0.1 g). [f] Amount of adsorbed *n*-butylamine per gram of the catalyst after stirring 200 mL of aqueous *n*-butylamine solution (0.25 M) with 0.1 g of the catalyst for 24 h in the dark. The amount of adsorbed *n*-butylamine was estimated from the nitrogen content in the adsorbent measured by elemental analysis.

clearly shows that spontaneous water intercalation to $K_2La_{2/3}Ta_2O_7$ occurs more rapidly. Hence, it is reasonable to assume that the interlayer electrostatic interaction of $K_2La_{2/3}Ta_2O_7$ is weaker than that of $K_2SrTa_2O_7$.

The XRD patterns showed that the structure of $H_2La_{2/3}Ta_2O_7$ (*P*4/*mmm*, $a = 3.9484$ Å, $c = 9.7742$ Å) is essentially the same as that of the hydrous form of $K_2La_{2/3}Ta_2O_7$ as well as that of $H_2SrTa_2O_7$ (*P*4/*mmm*, $a = 3.9038$ Å, $c = 9.7742$ Å). The hydration number was estimated from a weight loss in the TGA analysis below 743 K, which could be due to the transformation of the hydrate to the anhydrous layered material. The hydration numbers in the formula of $K_2La_{2/3}Ta_2O_7 \cdot nH_2O$ and $H_2La_{2/3}Ta_2O_7 \cdot nH_2O$ were 2.1 and 1.0, respectively (Table 1).

Figure 1g shows an XRD pattern of the sample obtained by complete dehydration of $H_2La_{2/3}Ta_2O_7$ at 1273 K for 6 h. The (*hk*0) reflections of $H_2La_{2/3}Ta_2O_7$ characteristic to the layered perovskite structure are lost. Most of the lines observed are assigned to the perovskite $La_{1/3}TaO_3$ (JCPDS 42-0061) in which two-thirds of the A-cation sites are vacant. This indicates that the condensation of terminal OH groups to form Ta−O−Ta linkages between layers and motion of La^{3+} into the perovskite A-sites resulted in a transformation of the two-dimensional layered structure into a three-dimensional phase, as observed in similar Ruddlesden−Popper systems.[17]

UV−vis spectra of the catalysts are shown in Figure 3. All the samples show an absorption band in the ultraviolet

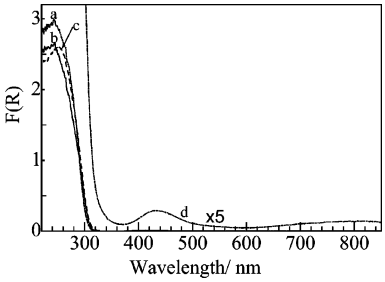

Figure 3. Diffuse reflectance UV−vis spectra of (a) $K_2La_{2/3}Ta_2O_7$, (b) $H_2La_{2/3}Ta_2O_7$, (c) $La_{1/3}TaO_3$, and (d) NiO(2 wt %)−$H_2La_{2/3}Ta_2O_7$.

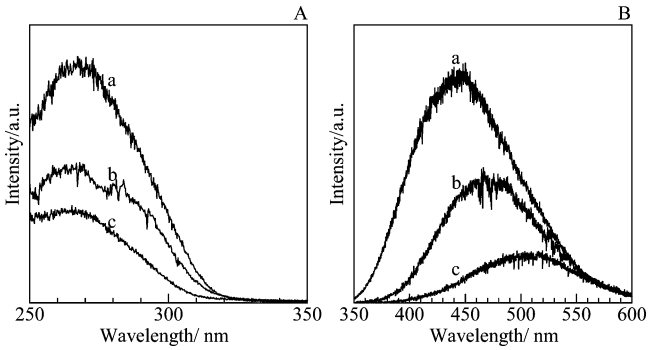

Figure 4. (A) Excitation and (B) emission spectra of (a) anhydrous $K_2La_{2/3}Ta_2O_7$, (b) $K_2La_{2/3}Ta_2O_7$, and (c) $H_2La_{2/3}Ta_2O_7$ measured at 77 K. Excitation for emission spectra, 290 nm; monitoring emission for excitation spectra, 490 nm.

region and show a clear absorption edge at around 310−320 nm. From the absorption edge, the band gap of $K_2La_{2/3}Ta_2O_7$, $H_2La_{2/3}Ta_2O_7$, and $La_{1/3}TaO_3$ is 4.0 eV, and that of $H_2SrTa_2O_7$ is 3.9 eV. Figure 4 shows emission and excitation spectra of the layered tantalates.

In the emission spectra with an excitation wavelength of 290 nm, the anhydrous $K_2La_{2/3}Ta_2O_7$ showed an intense luminescence peak with a maximum around 440 nm. Although the luminescence properties of this compound were not reported, the positions of the excitation and emission peaks are very close to those of other anhydrous perovskite tantalates, such as $KTaO_3$ and $Sr_2Ta_2O_7$.[19−21] The excitation and emission transitions are known to be due to charge-transfer transitions within the octahedral tantalate groups.[19] The hydrous $K_2La_{2/3}Ta_2O_7$ and $H_2La_{2/3}Ta_2O_7$ showed a weaker band with a maximum around 420 and 500 nm, respectively. These results can be interpreted that the photoluminescence intensity of the layered tantalates are decreased when the interlayer water is present. The onsets of the excitation spectra (310−320 nm) coincide with the onsets of the UV−vis spectra, indicating that photogenerated electrons and holes play a role in the emission. It is reasonable to assume that in the hydrated layered tantalates photogenerated electrons and holes can be readily transferred to the interlayer water. Hence, we consider that the low luminescence efficiency of the hydrous forms is mainly due to the electron and/or hole transfer to the interlayer water rather than the nonradiative transition. Among the hydrates,

(19) Srivastava, A. M.; Ackerman, J. F.; Beers, W. W. *J. Solid State Chem.* **1997**, *134*, 187.
(20) Weigel, M. J.; Emond, M. H.; Stobbe, E. R.; Blasse, G. *J. Phys. Chem. Solids* **1994**, *55*, 773.
(21) Blasse, G.; Brixner, L. H. *Mater. Res. Bull.* **1989**, *24*, 363.

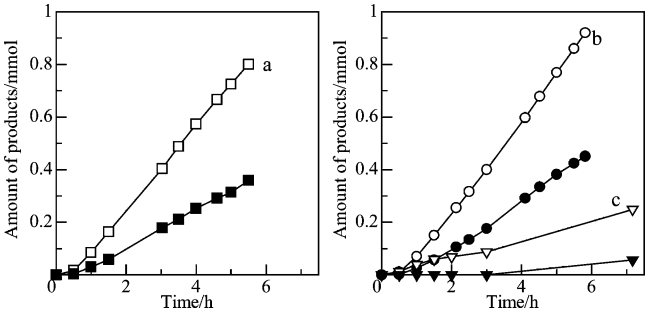

Figure 5. H_2 (open symbols) and O_2 (closed symbols) evolutions from distilled water with (a) $K_2La_{2/3}Ta_2O_7$, (b) $H_2La_{2/3}Ta_2O_7$, and (c) $La_{1/3}TaO_3$ under UV light (400 W high-pressure Hg lamp). The catalyst amount is 0.5 g.

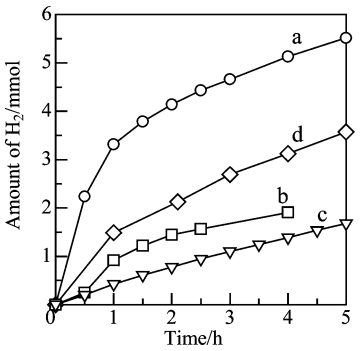

Figure 6. H_2 evolution from an aqueous *n*-butylamine (0.25 M) solution over (a) $H_2La_{2/3}Ta_2O_7$, (b) $K_2La_{2/3}Ta_2O_7$, (c) $La_{1/3}TaO_3$, and (d) $H_2SrTa_2O_7$. The catalyst amount is 0.1 g.

$H_2La_{2/3}Ta_2O_7$ showed lower photoluminescence intensity than $K_2La_{2/3}Ta_2O_7$. This may be caused by the lower crystallinity of the former sample as shown by the XRD result in Figure 1.

Effect of the Hydrous Interlayer on the Photocatalytic Activity. A time course of gas evolution for the photocatalytic decomposition of water over $K_2La_{2/3}Ta_2O_7$, $H_2La_{2/3}Ta_2O_7$, and $La_{1/3}TaO_3$ is shown in Figure 5. The rates of gas evolution on various Ta-based catalysts are listed in Table 1, together with the activity of $H_2SrTa_2O_7$[13] and $KTaO_3$ reported in our previous study. Novel photocatalysts, $K_2La_{2/3}Ta_2O_7$ and $H_2La_{2/3}Ta_2O_7$, produce H_2 and O_2 in a stoichiometric ratio ($H_2/O_2 = 2/1$), and the reaction proceeded at a steady rate. It is clear that hydrous layered tantalates show higher rates of H_2 and O_2 formation than anhydrous perovskites, $KTaO_3$ and $La_{1/3}TaO_3$. Considering the photoluminescence result (Figure 4) suggesting electron and/or hole transfer to the interlayer water, the positive effect of the hydrated interlayer on the activity could be explained as follows. The photogenerated electrons and holes can be effectively transferred to the interlayer water, resulting in the effective photocatalytic water splitting.

In overall water splitting, oxidation of water by holes is a slower process than reduction by electrons. To facilitate the oxidation, hole-scavengers are often introduced. In this study, *n*-butylamine was used as a sacrificial agent. Figure 6 shows the time course of H_2 evolution from an aqueous solution of *n*-butylamine (0.25 M). For all the catalysts tested, the initial rate of H_2 formation (Table 1) was higher than that in the absence of *n*-butylamine. The results in Table 2 show that the activity sequence for the *n*-butylamine/H_2O system

Table 2. Physical Properties and Photocatalytic Activities of Various Perovskite-Type Tantalates

catalyst[a]	state of Ni[b]	SBET $m^2\ g^{-1}$ [c]	evolution rate (mmol h^{-1}) H_2[d]	O_2[d]
NiO(2 wt %)−$H_2La_{2/3}Ta_2O_7$	Ni^{2+}, NiO cluster	16.7	940	459
NiO(0.5 wt %)−$H_2SrTa_2O_7$	NiO particle	4.7	240	59

[a] Amount of NiO loaded is in parentheses. [b] Estimated from XAFS and UV−vis results. [c] BET surface area. [d] Rate of H_2 or O_2 evolution from pure water (catalyst amount = 0.5 g).

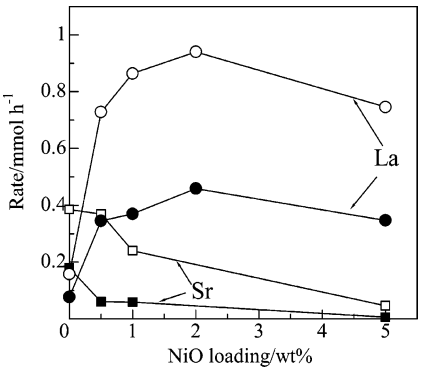

Figure 7. Effect of NiO loading on H_2 (open symbols) and O_2 (closed symbols) evolution rates over NiO−$H_2La_{2/3}Ta_2O_7$ or NiO−$H_2SrTa_2O_7$. The catalyst amount is 0.5 g.

($H_2La_{2/3}Ta_2O_7 > K_2La_{2/3}Ta_2O_7$) is markedly different from that observed in the H_2 evolution from pure water ($H_2La_{2/3}Ta_2O_7 \approx K_2La_{2/3}Ta_2O_7$). It is well-known that H^+-exchanged layered oxides can intercalate organic bases such as amines into the interlayer space.[18,22] Table 2 includes the amount of *n*-butylamine adsorbed on the samples when the sample was stirred in the dark for 24 h under the same condition as the catalytic reaction. The amount of *n*-butylamine adsorbed on $H_2La_{2/3}Ta_2O_7$ is 0.90 mmol g^{-1} (0.51 mol/mol) and is larger than that on $K_2La_{2/3}Ta_2O_7$ (0.38 mmol g^{-1}, 0.21 mol/mol). Therefore, the higher activity of $H_2La_{2/3}Ta_2O_7$ for the *n*-butylamine/H_2O system can be caused by the effective consumption of the hole present at the surface of the perovskite sheet via its reduction with intercalated *n*-butylamine. This supports the above proposal that the photocatalytic reaction proceeds at the interlayer of the hydrated layered tantalates.

Photocatalytic Activity of Ni-Loaded $H_2ATa_2O_7$ (A = $La_{2/3}$, Sr). The rates of H_2 and O_2 evolutions over $H_2La_{2/3}Ta_2O_7$ were significantly increased by the addition of Ni as a cocatalyst (Figure 7). The activity increased steeply with 0.5 wt % of NiO, reached a maximum at a content of 2 wt %, and decreased slightly with a larger amount of NiO. In contrast, Ni loading resulted in a decrease in the activity of $H_2SrTa_2O_7$. Consequently, the H_2 formation rates of NiO−$H_2La_{2/3}Ta_2O_7$ samples are higher than those of NiO−$H_2SrTa_2O_7$. A similar result was also obtained for K-exchanged catalysts: the H_2 formation rate of NiO(0.5 wt %)−$K_2La_{2/3}Ta_2O_7$ (262 μmol h^{-1}) was higher than that of NiO(0.5 wt %)−$H_2SrTa_2O_7$ (67 μmol h^{-1}). NiO−$H_2La_{2/3}Ta_2O_7$ (NiO = 2 wt %) produced stoichiometric mixtures of H_2 and O_2 with steady-state rates, and the rates of H_2 and O_2 formation were

(22) Ebina, Y.; Tanaka, A.; Kondo, J. N.; Domen, K. *Chem. Mater*. **1996**, *8*, 2534.

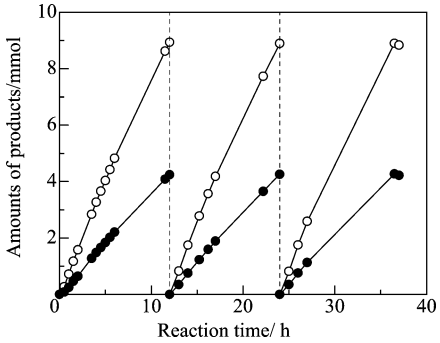

Figure 8. H_2 (open circles) and O_2 (closed circles) evolutions from distilled water over NiO(1 wt %)−$H_2La_{2/3}Ta_2O_7$. The catalyst amount is 0.5 g.

940 and 459 μmol h^{-1}, respectively. These values are 6 times higher than those of unmodified $H_2La_{2/3}Ta_2O_7$. With the use of the NiO−$H_2La_{2/3}Ta_2O_7$ (NiO = 1 wt %), the reaction was performed for a long period (Figure 8). After the first run, the system was evacuated, and the reaction was repeated using the same reaction mixture. In the second and third runs, the overall splitting of water occurred with almost the same rate as that of the first run, which demonstrates a high durability of the catalyst. The total amount of H_2 evolved during these runs reached 30 mol (mol cat.)$^{-1}$, indicating that overall water splitting on this material proceeds catalytically.

Characterization of Ni-Loaded $H_2ATa_2O_7$ (A = $La_{2/3}$, Sr). The structure of the Ni species in Ni-loaded samples was well-characterized by a combination of XRD, TEM, UV−vis spectroscopy, and Ni K-edge XANES/EXAFS. XRD patterns of Ni-loaded samples show no lines due to NiO or metallic Ni. Because of the cation-exchanging ability of $H_2La_{2/3}Ta_2O_7$, the H^+/Ni^{2+} cation exchange in the impregnation process should result in an intercalation of hydrated Ni^{2+} ions at the cation-exchange site in the interlayer. The UV−vis spectrum of uncalcined Ni^{2+}−$H_2La_{2/3}Ta_2O_7$ (result not shown) exhibited d−d transition bands of Ni^{2+} ion (390 nm and 650−750 nm), which confirms the presence of Ni^{2+} at the cation-exchange site in the interlayer. As shown in Figure 3, the d−d transition bands of Ni^{2+} ion (430 nm and 750−900 nm) were also observed in the UV−vis spectrum of NiO−$H_2La_{2/3}Ta_2O_7$, indicating that the cationic state of the intercalated Ni^{2+} remained after calcination at 573 K. In the EXAFS spectrum of NiO−$H_2La_{2/3}Ta_2O_7$, a small peak assignable to the Ni−Ni shell in the oxide is observed (Figure 9B). The relative peak intensity of the Ni−Ni shell against that of the Ni−O bond is much smaller than that of NiO. The curve-fitting analysis shows that the peaks due to the first and the second coordination sphere of Ni can be assigned to 4.5 Ni−O bonds with a distance of 1.98 Å and 0.9 Ni−Ni shells with a distance of 3.07 Å. These values are clearly different from those of NiO. As shown in Figure 9A, the XANES feature of NiO−$H_2La_{2/3}Ta_2O_7$ is different from those of NiO but rather close to that of $Ni(OAc)_2{\cdot}6H_2O$. The EXAFS analysis of NiO−$H_2SrTa_2O_7$ shows that the coordination number for the second neighboring Ni atom (CN = 4.0) is larger than that for NiO−$H_2La_{2/3}Ta_2O_7$, and its Ni−Ni distance (2.97 Å) is very close to that of NiO (2.95 Å). The position of the intense XANES peak of NiO−$H_2SrTa_2O_7$ (8349.5 eV) is the same as that of NiO.

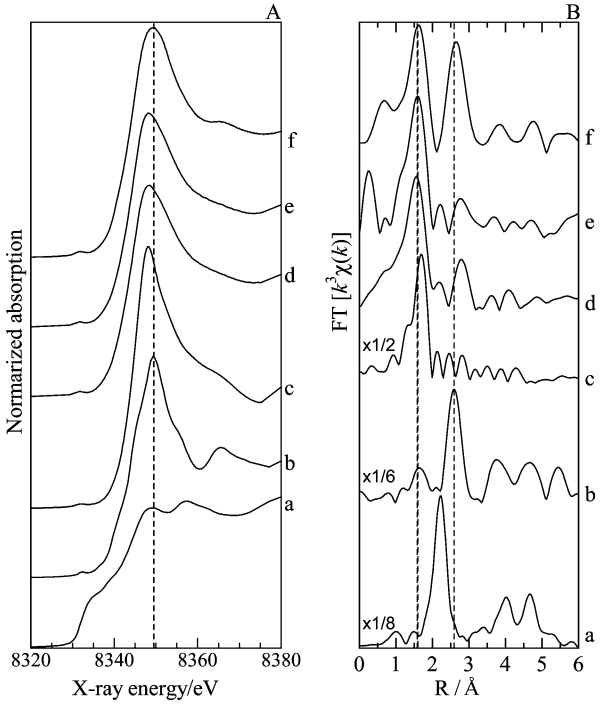

Figure 9. (A) Ni K-edge XANES spectra and (B) Fourier transforms of k^3-weighted EXAFS oscillation (phase shift uncorrected) for (a) Ni foil, (b) NiO, (c) $Ni(OAc)_2{\cdot}6H_2O$, (d) NiO(2 wt %)−$H_2La_{2/3}Ta_2O_7$, (e) NiO(2 wt %)−$H_2La_{2/3}Ta_2O_7$ after photocatalytic water splitting for 5 h, and (f) NiO(0.5 wt %)−$H_2SrTa_2O_7$.

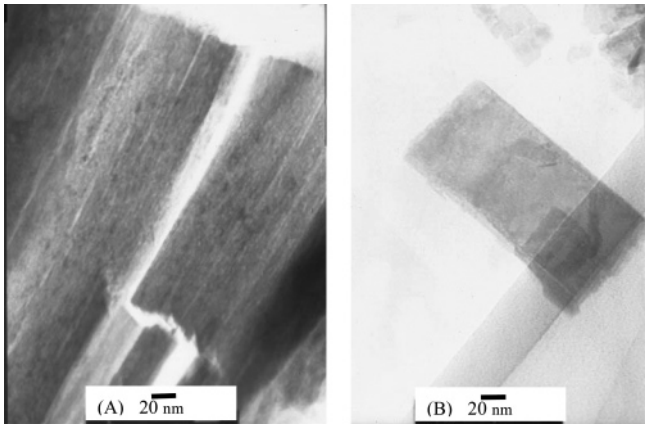

Figure 10. TEM images of NiO(2 wt %)−$H_2La_{2/3}Ta_2O_7$ taken from the direction (A) parallel with and (B) perpendicular to the basal plane of $H_2La_{2/3}Ta_2O_7$.

Figure 10, parts A and B, shows TEM images of NiO−$H_2La_{2/3}Ta_2O_7$ (NiO = 2 wt %) taken from the direction parallel with and perpendicular to the basal plane of $H_2La_{2/3}Ta_2O_7$, respectively. NiO particles located at the outer surface of the perovskite are scarcely observed. The XRD result in Figure 1 shows no increase in the interlayer distance of $H_2La_{2/3}Ta_2O_7$ after Ni loading. However, nitrogen adsorption experiments showed that the surface area of NiO−$H_2La_{2/3}Ta_2O_7$ is 3 times higher than that of $H_2La_{2/3}Ta_2O_7$, which suggests the pillaring of small NiO clusters in NiO−$H_2La_{2/3}Ta_2O_7$. The TEM photograph (Figures 10A) exhibits many cleavages running along the layer. This may be a possible reason for the increased surface area, whereas the surface area of $H_2SrTa_2O_7$ did not increase after the introduction of

Table 3. Ni K-Edge EXAFS Analysis

sample	shell	CN	*R* Å	σ^2 Å^2
NiO−$H_2La_{2/3}Ta_2O_7$	O	4.5	1.98	0.055
	Ni	0.9	3.07	0.055
NiO−$H_2La_{2/3}Ta_2O_7$ (after reaction)	O	5.0	2.01	0.068
	Ni	1.0	3.07	0.082
NiO−$H_2SrTa_2O_7$	O	4.0	2.01	0.044
	Ni	4.0	2.97	0.088
NiO	O	(6)[a]	(2.09)[a]	
	Ni	(12)[a]	(2.95)[a]	

[a] Data in parentheses are crystallographic data.

NiO (Table 3). Summarizing the above results, we conclude that the Ni species in NiO−$H_2La_{2/3}Ta_2O_7$ are Ni^{2+} cations and NiO clusters present at the interlayer. The size of the intercalated NiO cluster should be below nanometer order and/or it is the minor Ni species, because the XRD and TEM results suggest no detectable increase in the interlayer distance. On the other hand, the main Ni species in NiO−$H_2SrTa_2O_7$ are larger NiO particles possibly located at the external surface of $H_2SrTa_2O_7$. Generally, the higher NiO loading results in the larger particle size of NiO. Our characterization results show that NiO dispersion for NiO(2 wt %)−$H_2La_{2/3}Ta_2O_7$ is higher than that for NiO(0.5 wt %)−$H_2SrTa_2O_7$, although the NiO loading of the former sample is larger than the latter sample. Taking into account the fact that water intercalation into $K_2La_{2/3}Ta_2O_7$ proceeded more rapidly than it did into $K_2SrTa_2O_7$, probably due to a weaker interlayer electrostatic interaction of $K_2La_{2/3}Ta_2O_7$, the difference in the structure of the two Ni-loaded catalysts can be explained as follows. During the calcination of NiO−$H_2SrTa_2O_7$, a strong electrostatic force of attraction between perovskite layers make the neutral NiO species migrate to the external surface. A weaker interlayer electrostatic interaction in NiO−$H_2La_{2/3}Ta_2O_7$ should retard such a phenomenon. The TEM image of NiO−$H_2La_{2/3}Ta_2O_7$ does not essentially change after the reaction (not shown). The state of the Ni species in NiO−$H_2La_{2/3}Ta_2O_7$ does not markedly change after the reaction; the XANES feature and structural parameters from EXAFS analysis for NiO−$H_2La_{2/3}Ta_2O_7$ did not markedly change after the catalyst was photoirradiated under the standard photocatalytic water splitting condition for 5 h (Figure 9, Table 3). These indicate that the aggregation of Ni species or migration of Ni to the external surface of $H_2La_{2/3}Ta_2O_7$ does not occur during the reaction.

Taking into account the reaction results that Ni loading on $H_2La_{2/3}Ta_2O_7$ significantly increased its photocatalytic activity, while Ni loading did not improve the activity of $H_2SrTa_2O_7$, the above structural results indicate that highly dispersed Ni(II) species at the interlayer space act as active sites for H_2 formation, while large NiO particles on the external surface of $H_2SrTa_2O_7$ do not participate in the reaction. The structural model shown in Figure 11 explains

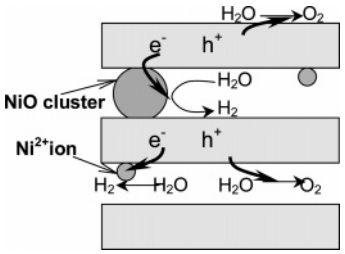

Figure 11. Schematic view of the reaction mechanism of water splitting on NiO−$H_2La_{2/3}Ta_2O_7$.

the higher photocatalytic efficiency of NiO−$H_2La_{2/3}Ta_2O_7$ than that of NiO−$H_2SrTa_2O_7$. If the Ni site as a water reduction site[1,3−10] is present between hydrous tantalate sheets with a nanometer order thickness, photogenerated electrons in the tantalate sheets can be easily migrated to the Ni sites to reduce intercalated water. Simultaneously, the oxidation of intercalated water by holes occurs at the surface of the perovskite sheets (TaO_6 sites). Hence, as previously proposed for the NiO_x-intercalated niobate photocatalyst,[4] the electron−hole recombination process in the NiO−$H_2La_{2/3}Ta_2O_7$ catalyst could be retarded by physical separation of the electron and hole pairs. As for NiO−$H_2SrTa_2O_7$, the NiO site present at the external surface of perovskite should not act as a H_2 formation site, because a long-distance diffusion of photogenerated electrons is needed. In addition, the presence of NiO at the external surface should decrease the activity of $H_2SrTa_2O_7$ because of photoabsorption by NiO inhibits the photoexcitation of the perovskite.

In summary, we have presented a series of novel photocatalysts based on $n = 2$ members of Ruddlesden−Popper-type hydrous layered tantalates, $A'_2ATa_2O_7$ ($A' = H$ or K, $A = La_{2/3}$ or Sr) for the water splitting into H_2 and O_2 under UV irradiation. Intercalation of Ni(II) species (Ni^{2+} cations and NiO clusters) into the perovskite layers of $H_2La_{3/2}Ta_2O_7$ improves the activity. The high activity of the NiO−$H_2La_{2/3}Ta_2O_7$ catalyst could be due to a short-distance migration of photogenerated electrons and holes to the adjacent Ni(II) and surface TaO_6 sites, respectively, and a resulting separation of the electron and hole pairs. This is the first successful example of highly active metal-intercalated layered tantalate photocatalysts with hydrated interlayer space.

Acknowledgment. The X-ray absorption experiments were performed under the approval of the Photon Factory Program Advisory Committee (Proposal No. 2003G-274). The authors thank Mr. S. Komai of Nagoya University for his help in the TEM experiment. This work was supported by the Solution Oriented Research for Science and Technology (SORST) program from the Japan Science and Technology Corporation (JST).

CM050982C